https://doi.org/10.5194/egusphere-2026-702
Preprint. Discussion started: 9 March 2026

Daily maps of Boundary Layer Height combining radiosonde, satellite, and reanalysis over Europe

Carina I. Argañaraz[1,2], Andreu Salcedo-Bosch[3], Simone Lolli[3], Gabriele Curci[1,2]

[1] Department of Physical and Chemical Sciences, Università degli Studi dell'Aquila, Via Vetoio, 67100 L'Aquila, Italy.

[2] Center of Excellence in Telesensing of Environment and Model Prediction of Severe events (CETEMPS), Università degli Studi dell'Aquila, Via Vetoio, 67100 L'Aquila, Italy.

[3] CNR-IMAA, Contrada S. Loja snc, 85050 Tito Scalo (PZ), Italy.

Correspondence to: carinaines.arganaraz1@univaq.it

Abstract

The height of the planetary boundary layer directly influences local and regional climatic phenomena, making its study and estimation of vital importance for environmental sciences. The main objective of this work was to create a gridded map of planetary boundary layer height across the European continent, with a spatial resolution of 25 km and monthly mean values at two synoptic hours (12:00 and 00:00 UTC). We implemented the regression kriging method by combining various data sources, including observations, climatic and topographic variables, and reanalysis data (ERA5), and different regression methods (linear, random forest, and gradient boosting) for the 2010-2020 period. In both UTC hours, combining reanalysis and topographic covariates with random forest regression provided the best performance. Then, we compared our seasonal predictions with reanalysis data and found a consistently higher spatio-temporal accuracy than that of the ERA5 reanalysis. For example, at 12:00 UTC, spatial variability in winter showed RMSE values ≤ 100 m, compared with ≥ 200 m for ERA5, while temporal variability in summer reached RMSE values ≤ 250 m, versus ≥ 300 m for ERA5. At 00:00 UTC, spatial variability in autumn achieved RMSE values ≤ 36 m, whereas ERA5 exhibited RMSE values ≥ 130 m.

The methodology was applied to a case study over Germany at a daily resolution. We obtained an accurate representation of boundary layer height, which was consistent with the variations in weather conditions. Results were notably better at 12:00 than at 00:00 UTC, mainly due to the limited number of available stations and the associated difficulty in resolving the stable boundary layer at night. Overall, this study represents a promising first step towards the incorporation of this type of data in atmospheric models with the aim of reducing the bias in boundary layer height simulation.

Keywords Modelling, ERA5, DEM, MODIS, E-OBS, Interpolation

https://doi.org/10.5194/egusphere-2026-702
Preprint. Discussion started: 9 March 2026

1. Introduction

The Boundary Layer (BL) is the lowest part of the troposphere in contact with the Earth's surface, responding on short time scales to surface atmosphere exchanges of heat fluxes, solar radiation, pollutant emissions, moisture, momentum, land cover, and topography. The dynamics of the BL are strongly influenced by the diurnal cycle. Consequently, two contrasting situations can be observed in terms of BL characteristics. During the day, a deeper and more turbulent convective boundary layer (CBL) develops, driven by convective thermals generated by sensible and latent heat fluxes. In contrast, after sunset, radiative cooling of the ground or the advection of warm air over a colder surface leads to the formation of a shallow and less turbulent stable boundary layer (SBL) at night (Stull 1988).

The height of the boundary layer (BLH), that is, how deep it can become during the day and how shallow it remains at night, represents a key parameter in meteorology and is typically defined as the altitude of the inversion layer that separates the free atmosphere from the planetary boundary layer (Stull 1988). Its top defines many tropospheric processes that influence climate and air quality, such as the transport, transformation, and mixing of aerosols and pollutants (Seibert et al., 2000; Zhang et al., 2013). Therefore, the role of BLH in climatological processes and in sustaining a healthy environment for human life makes its study a highly relevant topic in environmental sciences.

In practice, estimating the BLH at different times of the day is a real challenge, as it results from a multitude of processes acting simultaneously across a wide range of spatial and temporal scales. The factors influencing its estimation may vary across different regions of the Earth. For instance, solar radiation strongly drives latitudinal differences, with greater BLH values at mid- and low latitudes compared to higher latitudes (Guo et al., 2021).

Seasonality also plays a key role: in some regions, BLH tends to be higher in spring and summer, and generally lower in autumn and winter (Guo et al., 2019; Saha et al., 2022). In other regions, however, it reaches its greatest depth in summer and its shallowest extent in winter, with transitional values observed in spring and autumn (Nelson et al., 2021; Li et al., 2023). Seasonal rainfall patterns and dry periods exert a strong influence on BLH as well, directly modulating its variability (Dias-Júnior et al.,

https://doi.org/10.5194/egusphere-2026-702
Preprint. Discussion started: 9 March 2026

2022; Li et al., 2023). At higher altitudes, however, this seasonal pattern may be reversed, since topography is another critical driver of BLH (De Wekker and Kossmann 2015).

Regardless of the inherent complexity and variability described above, BLH estimation also varies depending on the mathematical approaches applied and the diversity of instruments used to obtain the input data. These factors introduce biases among the different procedures implemented to determine BLH (Seibert et al., 2000; Chen et al., 2023; Roldán-Henao et al., 2024; Zhang et al., 2025). Most methods for calculating the top of the BL rely on vertical profiles of climatic variables, including temperature, pressure, wind, humidity, water vapor, and refractive index (Seibert et al., 2000; Seidel et al., 2010). In practice, these profiles can be obtained from radiosondes or ground-based remote sensing instruments (e.g., LIDAR, SODAR, microwave radiometers, among others). Alternatively, BLH estimates can be obtained from reanalysis products (Seibert et al., 2000; Guo et al., 2021; Saha et al., 2022).

Reanalysis products are a powerful tool with notable advantages over other approaches. They combine real-world observations with numerical model forecasts and data assimilation. This integration provides consistent estimates of atmospheric, surface, and oceanic parameters for all locations worldwide, with no spatial gaps (Teixeira et al., 2021). Numerous studies have evaluated the efficiency with which reanalysis can reproduce the daily dynamics of the boundary layer. Evidence indicates that the BLH from ERA5 (the fifth-generation ECMWF reanalysis) is reliable when compared with observational datasets, showing correlations close to $r = 0.9$ and biases ranging from a few metres to more than one kilometre. Nonetheless, findings also reveal systematic underestimations or overestimations of BLH from ERA5 at specific times of day and the study region (Guo et al., 2021; Sinclair et al., 2022; Dias-Junior et al., 2022; Slättberg et al., 2022; Li et al., 2023).

Recent advances in modelling approaches that integrate observations, remote sensing data, and reanalysis to predict BLH values have yielded promising results (Ayazpour et al., 2023; Guo et al., 2024; Zhang et al., 2025). This progress highlights the inherent complexity of the numerous processes operating simultaneously across a wide range of spatial and temporal scales. In this context, the continuous spatio-temporal coverage provided by reanalysis is particularly valuable (Sinclair et al., 2022; Guo et al., 2024). Its application to the generation of gridded maps, in combination with other variables, enables the production of more refined BLH representations (Ayazpour et al.,

https://doi.org/10.5194/egusphere-2026-702
Preprint. Discussion started: 9 March 2026

2023). By offering a more accurate baseline for analysing BLH trends and variability, including their climatic impacts, these products may serve as a reference for evaluating regional climate models and for the development of high-resolution regional climate change scenarios.

To this end, the present study pursues the following objectives: (1) building a gridded map of BLH across Europe using observational BLH data from radiosondes (BLH_{RS}), combined with BLH derived from reanalysis (BLH_{ERA5}) and climatic and topographic variables; (2) evaluating the accuracy of the resulting observational gridded maps against observational data, both spatially and temporally; and (3) to apply the proposed methodology to a local case study and compare the result with reanalysis.

The remainder of this paper is structured as follows. 2-Data and Methodology describes the datasets and methods employed to create and evaluate the gridded maps. 3-Results section presents the performance of the gridded maps alongside the results of the case study. Finally, section 4 provides a discussion and section 5 the concluding remarks.

2. Data and Methodology

2.1 Study area and BLH from radiosonde

This study covers the European continent, encompassing diverse climatic and topographic regimes. The planetary boundary layer height (BLH_{RS}) radiosonde data employed here were derived from observations originally compiled in a previous work. Briefly, radiosonde data were collected between 2010 and 2020 from several weather station sources. For each launch, vertical profiles of wind, pressure, temperature, relative humidity, and dew-point temperature were extracted. These data were then processed to estimate BLH_{RS} using the bulk Richardson number method (see Salcedo-Bosh et al., 2025 for methodological details). Accordingly, our focus here is on the procedures applied to manage and process these data.

The dataset comprises 129 stations (Fig. 1a), which were filtered according to two specific times representing contrasting stages of the planetary boundary layer: 12:00 UTC (CBL) and 00:00 UTC (SBL). Therefore, it is assumed that each day provides one measurement for each of these times. To ensure data quality, only launch stations with at least 45% daily coverage, equivalent to more than 1,800 days of data per station, were retained for the analysis. Due to the sparse temporal coverage of the dataset, monthly mean BLH values were used for both assessment and interpolation. Figures 1b and 1c

https://doi.org/10.5194/egusphere-2026-702
Preprint. Discussion started: 9 March 2026

show the stations' location selected for each time, totalling 44 at 12:00 UTC and 39 at 00:00 UTC, respectively.

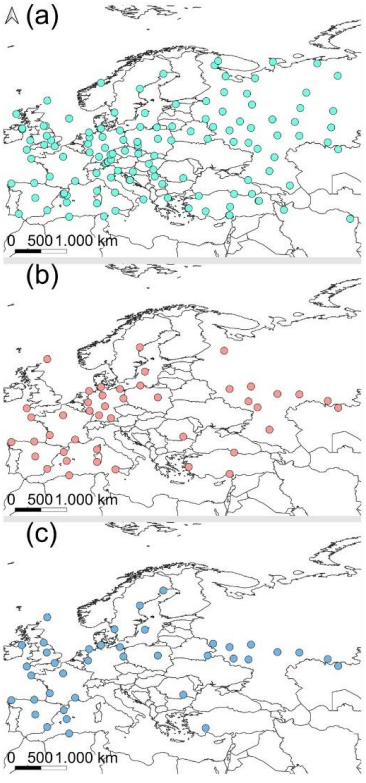

Figure 1 Map of the launch stations considered in the study. (a) Pool of stations available for the Europe region (12:00 UTC and 00:00 UTC). (b) 12:00 UTC stations with at least 45% of daily data for the 11 years (N = 44). (c) 00:00 UTC stations with at least 45% of daily data for the 11 years (N = 39).

2.2 Covariates

As our objective was to obtain an improved gridded map, the covariates selected were those related to boundary-layer development, directly or indirectly influencing the height of the capping inversion, and available as a gridded map. Below, we briefly describe the relevance and sources of the data considered in this study.

2.2.1 Reanalysis data

Among the products available, we used ERA5, as it has shown good correlation with BLH values derived from radiosondes (Guo et al., 2021, 2024; Sinclair et al., 2022). Although far from perfect, the accuracy of reanalysis products is often affected by

https://doi.org/10.5194/egusphere-2026-702
Preprint. Discussion started: 9 March 2026

seasonality (with larger errors during the warm months), topography, and other factors. Such discrepancies are frequently attributed to model parametrisations that do not accurately reflect real-world conditions (Guo et al., 2021; Dias-Júnior et al., 2022).

In ERA5, the boundary layer height (BLH_{ERA5}) is provided on a 1440 × 721 grid with a spatial resolution of 0.25° (approximately 25 km) in both latitude and longitude. It is calculated using the bulk Richardson number method, with a temporal resolution of one hour. We downloaded boundary layer height data from Copernicus Climate Service (https://cds.climate.copernicus.eu/datasets) at 12:00 UTC and 00:00 UTC for the full study period (2010-2020). BLH_{ERA5} values were then extracted for each station by matching date, hour, and latitude and longitude, with the nearest BLH_{ERA5} grid point assigned to each location. With these values, we calculate the monthly BLH_{ERA5} by station. Then we used the gridded map of monthly averages (11 years) at 12:00 and 00:00 UTC for the interpolation procedures.

2.2.2 Temperature and wind

Temperature plays a central role in the surface energy balance, which depends not only on solar radiation (e.g., the daily cycle) but also on soil moisture and land surface cover (Pal Arya 1988). Therefore, it is a powerful predictor of the spatio-temporal evolution of BLH (Guo et al., 2021; Madonna et al., 2021). Wind, in turn, is a fundamental component of the boundary layer, responsible for the horizontal and vertical transport of moisture, heat, momentum, and pollutants. Both variables are positively associated with BLH (Guo et al., 2016) and are also explicitly considered in BLH estimation methods (Seibert et al., 2000; Seidel et al., 2010). Hence, their inclusion as covariates is a natural choice.

2.2.2.1 Land surface temperature from satellite (MODIS)

MODIS (Moderate Resolution Imaging Spectroradiometer) is an instrument onboard NASA's Terra and Aqua satellites with different orbits. One of its products is Land Surface Temperature (LST) available at daily, 8-day, and monthly temporal resolutions, and at spatial resolutions of 1 km and 5 km. We compared the LST values from both satellites at each target time, given that the product is reported as 'daytime'/'night-time' rather than hourly data. Specifically, we examined how well Aqua (around 1:00 - 2:00 pm over Europe) versus Terra (~10:00 - 11:00 am) 'daytime' LST values aligned with BLH_{RS} at 12:00 UTC, and Aqua (1:00 - 2:00 am) versus Terra (~10:00 - 11:00 pm) 'night-time'

https://doi.org/10.5194/egusphere-2026-702
Preprint. Discussion started: 9 March 2026

LST values with BLH_{RS} at 00:00 UTC. This comparison allowed us to select the most suitable dataset for interpolation and further analysis.

We extracted LST values, Aqua (MYD11A1) / Terra (MOD11A1) (daytime and night-time) at 1 km spatial resolution for each radiosonde launch station and date. With these daily values, we calculate the monthly $LST_{Terra/Aqua}$ by station and UTC. For the interpolation procedure, we employed monthly mean LST data, extracted from Aqua (MYD21C3) and Terra (MOD21C3) (daytime and night-time) at 5 km resolution, which were subsequently resampled to 25 × 25 km^2 to match the resolution of ERA5 data. To ensure reliability, LST pixel values were filtered using data quality flags (bits 3 and 2), retaining only those with QA = 0 (good quality), since unreliable or unquantifiable pixels could bias the analysis. Consequently, we had some missing pixel data caused by cloud cover, poor input data, or calibration issues, which often resulted in fewer daily LST records than available in the observational dataset. All these steps were performed in Google Earth Engine.

2.2.2.2 Air temperature and wind speed from observation assemblage (E-OBS)

E-OBS (v31.0e) is an observation-based gridded dataset, available at daily temporal resolution and spatial resolutions ranging from 0.1° to 0.25°. The E-OBS gridded maps are produced by averaging 20 spatial simulations, each constructed using spatial correlations derived from the underlying observational network. As it is based on observational input, the spatial extent of E-OBS is more limited compared with that of other available products (e.g., LST). Accordingly, the study area when using this dataset is restricted to approximately 25°N-71.5°N latitude and 25°W-45°E longitude.

A priori, it was unclear which E-OBS product would be most representative. Specifically, whether daily mean or maximum temperature would best reflect BLH at 12:00 UTC, or whether daily mean or minimum temperature would be more appropriate for BLH at 00:00 UTC. To address this uncertainty, we downloaded all three available temperature products-daily mean temperature (TG), daily minimum temperature (TN), and daily maximum temperature (TX) -for a posteriori comparison- from https://surfobs.climate.copernicus.eu/dataaccess/access_eobs.php. Moreover, we downloaded daily mean wind speed (FG) data (Cornes et al., 2018).

We extracted the variable values by station using latitude-longitude and date; however, it should be noted that these values are daily, rather than hourly data (ERA5) or

https://doi.org/10.5194/egusphere-2026-702
Preprint. Discussion started: 9 March 2026

day/night segments (LST). Consequently, for the interpolation procedure, we employed monthly averages (11 years) for TG and FG, using the same gridded monthly maps for both 12:00 and 00:00 UTC interpolation. The spatial coverage of E-OBS slightly restricts our dataset, which extends further eastward in Europe, close to 50°E. As a result, fewer stations were available for the analyses.

2.2.3 Topography and geographic location

Landscape topography was considered as an additional covariate for BLH. The presence of valleys, basins, and plateaus interacts with mountain waves and thermally driven wind systems, thereby influencing BLH development (De Wekker and Kossmann 2015). Topography also directly affects the altitude starting point of the boundary layer.

Furthermore, geographic position may also be related to the intensity of thermal convection (Guo et al., 2021). However, the influence of geographical location (e.g., mid-latitude or tropical) on boundary layer evolution remains relatively unexplored (De Wekker and Kossmann 2015). Unlike the other covariates, coordinates and altitude do not exhibit daily variability and therefore correspond to constant values for each station.

2.2.3.1 Digital elevation model (DEM)

We extracted, for each station, the altitude values from the digital elevation model with 10 m of resolution available on https://dataspace.copernicus.eu/explore-data/data-collections/copernicus-contributing-missions/collections-description/COP-DEM. Then, the DEM was resampled to 25 x 25 km^2 of resolution for interpolation procedures.

2.2.3.2 Geographic location (Coords)

In our dataset, geographic coordinates were considered as covariates as was suggested by Hengl (2009). Latitude and longitude were transformed into plain coordinates (EPSG:3035) to estimate the deterministic component of the regression model and for the interpolation method (kriging).

2.3 Data management

First, we evaluated which temperature variable was best suited to each selected hour, namely Land Surface Temperature (Aqua and Terra) and the E-OBS air temperatures TG, TN, and TX. To this end, we applied regression kriging (further details in the *Interpolation Method* section) and compared the root mean standard error (RMSE) results, expressed as:

https://doi.org/10.5194/egusphere-2026-702
Preprint. Discussion started: 9 March 2026

$$RMSE = \sqrt{\frac{1}{N}\sum_{i=1}^{n}(y_i - \hat{y}_i)^2}$$

where y_i is the BLH_{RS}, and $\hat{y}_i$ is the predicted values by the model. The RMSE was obtained using a cross-validation (k-fold) procedure during training (explained in detail at the end of this section). Then, we compared the mean and std achieved with each temperature variable. The variable with the best performance was selected at each UTC.

We did not find significant differences among them (Figure A1); therefore, the option with the lowest monthly RMSE values was retained, specifically: TX and LST_{Aqua} at 12:00 UTC, and TG and LST_{Terra} at 00:00 UTC.

Once the temperature variables were selected in each case, we conducted exploratory correlations (both parametric and non-parametric) between all available covariates and BLH_{RS} values (monthly means by stations), to identify which covariates might be the most relevant and useful (Hengl 2009). For both UTC hours, the highest association was obtained with BLH_{ERA5} and the lowest with geographic coordinates (Table 1B).

To enable comparisons among the different parameters calculated in each section, a cross-validation procedure was performed during model training using the K-fold cross-validation function from the scikit-learn library. This approach allows the model to be evaluated using all available datasets by splitting the pool of stations into k consecutive folds. Each fold is then used once as the test set, while the remaining k - 1 folds are used for training.

When the number of stations (N) was ≥35, k was set to 5, resulting in five groups of seven sampling stations. Otherwise, when the number was smaller (N<35), k was set to 3. As the stations in the input dataset may be ordered according to geographical proximity, the shuffle option was applied to randomise the data before forming the folds. To ensure reproducibility, a fixed random seed was used. This procedure was applied in several sections of the manuscript and is hereafter referred to as cross-validation (K-fold).

2.4 Interpolation method

To perform the interpolation, we applied Regression Kriging (RK), a hybrid geostatistical method that combines classical spatial autocorrelation with secondary data (covariates) to define a background field for predicting the target variable. When input

https://doi.org/10.5194/egusphere-2026-702
Preprint. Discussion started: 9 March 2026

data are sparse, this approach is advantageous, as it provides additional support for the prediction (Krähenmann et al., 2018).

The regression component of RK models the relationship between the target variable (in our case, BLH_{RS}) and auxiliary environmental variables (covariates) at the sample locations. Once the deterministic part of the variation (regression) is estimated, the residuals, i.e., the variation not explained by the regression, can be interpolated using kriging and added to the estimated trend. The regression coefficients are obtained using Generalized Least Squares (GLS), which explicitly accounts for the spatial correlation among individual observations (more details on Hengl et al., 2007).

We implemented this method using the PyKrige package, which provides functions for combining kriging with both linear and non-linear regression models to fit the deterministic component. As shown in Table 1B, not all covariates exhibit a strong linear relationship with the target variable; in some cases, the values of Spearman's were similar or slightly higher than Pearson's. Therefore, we performed estimations using both parametric regression models, classical Linear Regression (LR) and non-parametric models, Random Forest (RF) and Gradient Boosting Forest (GB). For simplicity, and to minimise collinearity among covariates, we developed additive models including up to three predictor variables. BLH_{ERA5} was consistently retained as the core variable, as it has previously been used as a predictor of BLH from observation with good performance and relevance in the model (Ayazpour et al., 2023). The best-performing regression model for each covariate was selected based on a comparison of RMSE and MAE (mean absolute error) values obtained by cross-validation (k-fold) during training. Specifically, model values were compared using a one-way ANOVA (three factors corresponding to the regression models, with five replicates, $\alpha = 0.05$).

2.5 Interpolation assessment

To assess the performance of predictive models, three approaches were applied, cross-validation (RMSEr) and spatial-temporal validation, each for the respective time of day (12:00 and 00:00 UTC).

2.5.1 Cross-validation. To compare the accuracy of prediction between the models building with different covariates, we calculate the normalized root square error to compare between different models, through cross-validation (k-fold):

https://doi.org/10.5194/egusphere-2026-702
Preprint. Discussion started: 9 March 2026

$$RMSEr = \frac{\sqrt{\frac{1}{N}\sum_{i=1}^{n}(y_i - \hat{y}_i)^2}}{\theta_i}$$

where RMSEr is the RMSE pondered by the standard deviation (θ_i) of observed values. This parameter show how much of the global variation budget has been explained by the models.

The RMSEr was calculated for each model by month, followed by comparison of the average values and standard error. As a rule of thumb, a value of RMSEr that is close to 0.4 means a satisfactory accuracy of prediction (R^2 = 85%). Otherwise, if RMSEr > 0.7, this means that the model accounted for less than 50% of variability at the validation points (Hengl, 2009).

If the model error exceeds the intrinsic variability of the variable, the RMSEr value may be considerably greater than 1. The monthly values of each model were compared using ANOVA (by month, factors were the covariate models, with five replicates of RMSEr; $\alpha = 0.05$) to determine whether any of the combinations performed significantly better than the others.

2.5.2 Spatial validation. We compared the true prediction power using an independent (validation) data set. To perform this assessment, we considered launch stations that have at least the 45% of the data (11 yrs) for at least one month. Therefore, we found a new spatial point with a good representation of monthly data to compare with our best prediction assessed in a) for each UTC hour. A total of 20 validation stations (13 stations at 12:00 UTC, and 10 at 00:00 UTC) were considered, with 3 stations in common between the two timings (Figure A2). The predictive results were compared with the observed (BLH_{RS}) values and with the ERA5 boundary layer height data from Copernicus (henceforth blh_{ERA5}). Due to the low number of stations by calendar month, the comparison in this case, was purely qualitative.

2.5.3 Temporal validation. We compared the predicted values at the training stations against a subsequent temporal period (2021-2024). This approach was used to assess the coherence of the prediction obtained with respect to the input data at each location. Therefore, the predictive results (obtained with 2010-2020 data) and blh_{ERA5} (2021-2024) were compared with the BLH_{RS} from the 2021-2024 period. A linear mixed-effects model (GLMM) was fitted to assess the results across climatic seasons. BLH was specified as the response variable, the fixed factor was defined as the set of BLH sources (BLH_{RS},

https://doi.org/10.5194/egusphere-2026-702
Preprint. Discussion started: 9 March 2026

blh$_{ERA5}$, and the best-performing interpolated models), and the random factor was the stations. The analysis was implemented in Python using the 'statsmodels' package.

For assessments b and c, BLH values were plotted by UTC hour, models, and climatic season: winter (DJF), spring (MAM), summer (JJA), and autumn (SON). Statistically significant differences were indicated where applicable. In addition, the root mean square error (RMSE) was calculated for each climatic season and models to compare their performance against the observed values (BLH$_{RS}$).

3. Result

3.1 Regression models comparison

At 12:00 UTC (Table 1), Linear Regression (LR) and Random Forest (RF) show similar performance. Although the differences were not statistically significant, LR performed better for BLH$_{ERA5}$ and BLH$_{ERA5}$ + TX, while RF performed better for the remaining covariate combinations. Gradient Boosting (GB) showed the poorest performance for BLH$_{ERA5}$, BLH$_{ERA5}$ + FG, and BLH$_{ERA5}$ + DEM, and in general produced the highest error values and standard deviations. The best model fit obtained was BLH$_{ERA5}$ with an RMSE of 181 ± 81 m (mean ± std) and an MAE of 141 ± 68, achieved by LR.

At 00:00 UTC (Table 2), RF showed the best performance, reaching statistical significance in certain covariate combinations. It was followed by GB and, lastly, LR. The best results were the combination of BLH$_{ERA5}$ + DEM and BLH$_{ERA5}$ + DEM + Coordinates, which produced similar values: RMSE = 114 ± 6 m and MAE = 77 ± 10.

3.2 Interpolation assessment

3.2.1 Cross-validation

We compared the covariates' performances by month and UTC, calculating the RMSEr during training, through cross-validation (k-fold). At 12:00 UTC, the model including BLH$_{ERA5}$ + LST$_{Aqua}$ (obtained with RF) achieved the lowest monthly mean RMSEr = 0.61, showing a comparable performance to the model including also the Coords. These were followed by BLH$_{ERA5}$ + DEM + Coords (RF) (RMSEr = 0.67) and BLH$_{ERA5}$ (LR) (RMSEr = 0.68), the latter showing a similar performance to BLH$_{ERA5}$ + Coords (RF). Finally, the combination with topography, BLH$_{ERA5}$ + DEM (RF) reach up to 0.70.

https://doi.org/10.5194/egusphere-2026-702
Preprint. Discussion started: 9 March 2026

Overall, the models exhibited medium to poor monthly performance (RMSEr = 0.4-0.8), as shown in Figure A3. At 12:00 UTC, during the warmest months, RMSEr values ranged between 0.4 and 0.6, while in the coldest months the errors increased to 0.6-0.8. Although the monthly values produced by the models did not differ statistically, the model including LST achieved the best fit. Models including wind speed (FG) and maximum temperature (TX) yielded the worst performance and were therefore excluded from further comparison.

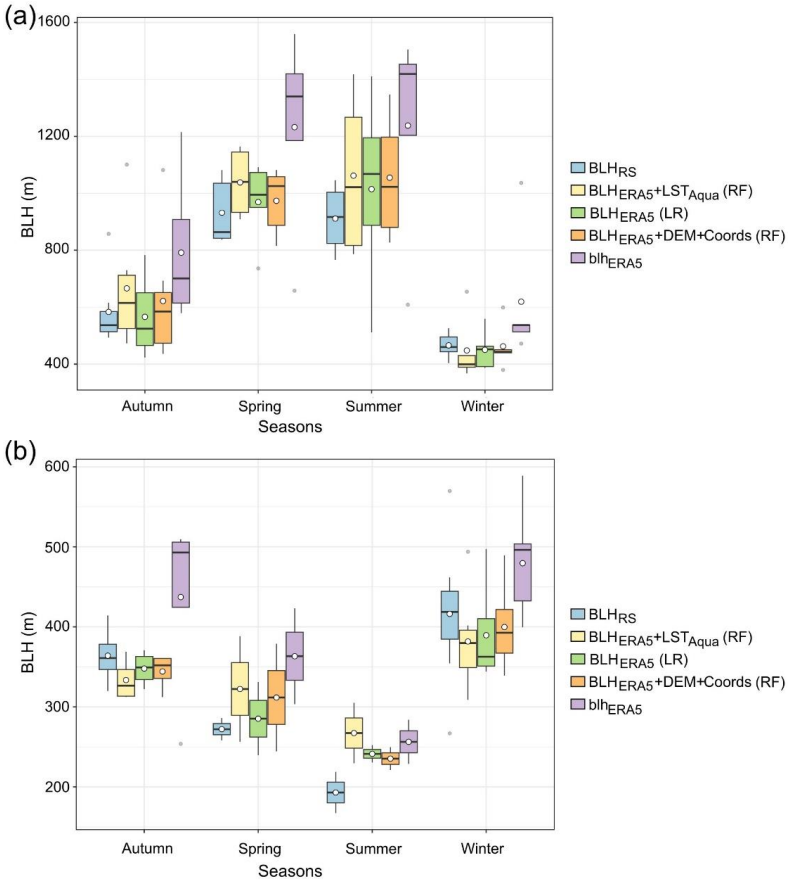

Figure 2 Boxplot of boundary-layer height from observation (BLH_{RS}), ERA5 (blh_{ERA5}), and from the interpolation models divided by seasons (2010-2020 yrs). (a) 12:00 UTC and (b) 00:00 UTC. Regression model in brackets. The boxes in each season/ hour are colour-coded according to the legend on the right side. The solid black line shows the median, and the white circles the mean values. The whiskers extend to the 5th and 95th percentiles. Grey circles beyond or above the whiskers show the outliers.

https://doi.org/10.5194/egusphere-2026-702
Preprint. Discussion started: 9 March 2026

At 00:00 UTC, the RMSEr values remained high, with the lowest value obtained for BLH_{ERA5} + LST_{Terra} (0.96), followed by BLH_{ERA5} (1.03) and BLH_{ERA5} + DEM + Coords (1.08), all of them obtained with RF. Consequently, for this UTC, a more flexible threshold for acceptable model performance was required. The monthly RMSEr values produced by the models did not differ statistically.

No clear seasonal effect was observed; instead, model performance remained relatively homogeneous throughout the year (Figure A3). However, the largest deviations were observed during summer. The best performance was achieved with the combinations including BLH_{ERA5} and LST_{Terra} ($0.3 \leq RMSEr \leq 1.2$). Models including wind speed (FG) and daily average temperature (TG) yielded the poorest performance and were therefore excluded from further analysis.

3.2.2 Spatial validation

At 12:00 UTC, the models that achieved the best performance in cross-validation, mentioned above, were subsequently used for comparisons with the observed values (BLH_{RS}) and those downloaded from Copernicus (blh_{ERA5}). As shown in Figure 2a, the predicted models performed closer to the observations during the autumn, spring, and winter seasons, whereas greater discrepancies were observed during the summer. These observations were in line with the RMSE values (Table 3), during the spring–summer seasons, the models exhibit an RMSE ≥ 162 m. In contrast, during winter the RMSE values decrease to less than 100 m for all three interpolation models. Moreover, the blh_{ERA5} values deviated the most from observations in all seasons, with a 230m < RMSE < 466 m. Overall, the best models were BLH_{ERA5} (LR) in winter and autumn, and BLH_{ERA5} + DEM + Coords (RF)in spring and summer. Showing better performance than those from blh_{ERA5} (Table 3).

At 00:00 UTC, the results obtained from the interpolation models were similar, as shown in Fig. 2b, with the model including LST_{Terra} and blh_{ERA5} product exhibiting the largest deviations from the observations (BLH_{RS}). In winter, the interpolation models showed the poorest agreement (RMSE ~ 65-77 m), whereas for blh_{ERA5}, the poorest performance occurred in autumn (RMSE = 132 m). The blh_{ERA5} values overestimated the observations across all seasons (45 m < RMSE < 132 m). Meanwhile, the interpolated estimates with the covariate BLH_{ERA5} had the best adjustment in winter, spring, and autumn, while BLH_{ERA5} + DEM + Coords in summer (Table 3). At both UTC, the model

https://doi.org/10.5194/egusphere-2026-702
Preprint. Discussion started: 9 March 2026

including LST showed poorer performance compared with the other two models, reflected in its higher dispersion values (Fig. 2a,b) and RMSE values (Table 3).

Table 1 RMSE and MAE (mean±std) results for the three regression models and covariate combination during the RK training process at 12:00 UTC. When the monthly mean values of the regression models differed significantly ($p \leq 0.05$), a Tukey post-hoc test was applied; different letters indicate statistically significant differences. The regression model with the lowest value was selected by covariate for the interpolation assessment (highlighted with *).

Covariates	Model	RMSE	MAE
BLH_{ERA5}	Linear Regression*	181±81[b]	141±68[b]
	Random Forest	185±79[b]	146±66[b]
	Gradient Boosting	303±128[a]	241±105[a]
BLH_{ERA5} + Coords	Linear Regression	182±56	146±53
	Random Forest*	181±56	142±51
	Gradient Boosting	214±84	163±66
BLH_{ERA5} + LST_{AQUA}	Linear Regression	212±74	182±66
	Random Forest*	233±79	165±59
	Gradient Boosting	265±87	201±68
BLH_{ERA5} + LST_{AQUA} + Coords	Linear Regression	234±79	282±66
	Random Forest*	212±74	195±59
	Gradient Boosting	265±87	202±68
BLH_{ERA5} + TX	Linear Regression*	205±80	161±60
	Random Forest	206±79	167±65
	Gradient Boosting	286±113	219±85
BLH_{ERA5} + TX + Coords	Linear Regression	194±78	155±57
	Random Forest*	194±70	155±55
	Gradient Boosting	244±91	182±65
BLH_{ERA5} + FG	Linear Regression	242±92	193±72[ab]
	Random Forest*	221±84	172±67[b]
	Gradient Boosting	336±175	279±151[a]
BLH_{ERA5} + FG + Coords	Linear Regression	242±89	189±71
	Random Forest*	219±79	168±61
	Gradient Boosting	264±119	207±93
BLH_{ERA5} + DEM	Linear Regression	220±74[b]	166±62[b]
	Random Forest*	198±59[b]	155±51[b]
	Gradient Boosting	318±112[a]	249±95[a]
BLH_{ERA5} + DEM + Coords	Linear Regression	210±60	164±55
	Random Forest*	193±59	152±55
	Gradient Boosting	234±93	181±76

https://doi.org/10.5194/egusphere-2026-702
Preprint. Discussion started: 9 March 2026

435

Table 2 Similar to Table 1 but using 00:00 UTC datasets

Covariate	Model	RMSE	MAE
BLH_{ERA5}	Linear Regression	127±6.0[b]	82±5.7[b]
	Random Forest*	125±5.0[b]	83±8.3[b]
	Gradient Boosting	173±13[a]	107±13[a]
BLH_{ERA5} + Coords	Linear Regression	130±6.3[b]	82±4.5[b]
	Random Forest*	126±4.3[b]	82 ±7.9[b]
	Gradient Boosting	164±11[a]	101±14[a]
BLH_{ERA5} + LST_{TERRA}	Linear Regression	137±12[ab]	92±8.3[a]
	Random Forest*	123±11[b]	84±10[a]
	Gradient Boosting	146±24[a]	96±18[a]
BLH_{ERA5} + LST_{TERRA} + Coords	Linear Regression	137±12[ab]	92±8.3[a]
	Random Forest*	122±11[b]	84±10[a]
	Gradient Boosting	145±24[a]	96±18[a]
BLH_{ERA5} + TG	Linear Regression	128±6.7	89±5.1
	Random Forest*	121±6.3	84±9.2
	Gradient Boosting	123±20	87±11
BLH_{ERA5} + TG + Coords	Linear Regression	152±15[a]	108±7.3[a]
	Random Forest*	121±6.5[b]	84±10[b]
	Gradient Boosting	122±19[b]	87±13[b]
BLH_{ERA5} + FG	Linear Regression	155±8.0[a]	114±8.4[a]
	Random Forest	129±10[b]	92±14[b]
	Gradient Boosting*	125±26[b]	91±25[b]
BLH_{ERA5} + FG + Coords	Linear Regression	165±13[a]	121±13[a]
	Random Forest*	129±9.1[c]	93.3±15[b]
	Gradient Boosting	149±14[b]	109±15[a]
BLH_{ERA5} + DEM	Linear Regression	132±7.7[a]	87±8.2[ab]
	Random Forest*	116±6.1[b]	78±10[b]
	Gradient Boosting	132±13[a]	92±16[a]
BLH_{ERA5} + DEM + Coords	Linear Regression	131±7.3[a]	88±6.3[a]
	Random Forest*	114±6.1[c]	77±10[b]
	Gradient Boosting	122±11[b]	84±11[ab]

3.2.3 Temporal validation

In this section, seasonal mean BLH_{RS} values (2021-2024 period) were compared
440 with blh_{ERA5} from the same period, as well as with estimates from models trained on the

https://doi.org/10.5194/egusphere-2026-702
Preprint. Discussion started: 9 March 2026

2010-2020 dataset. A generalised linear mixed model (GLMM) was applied to detect differences between the models and the radiosonde observations.

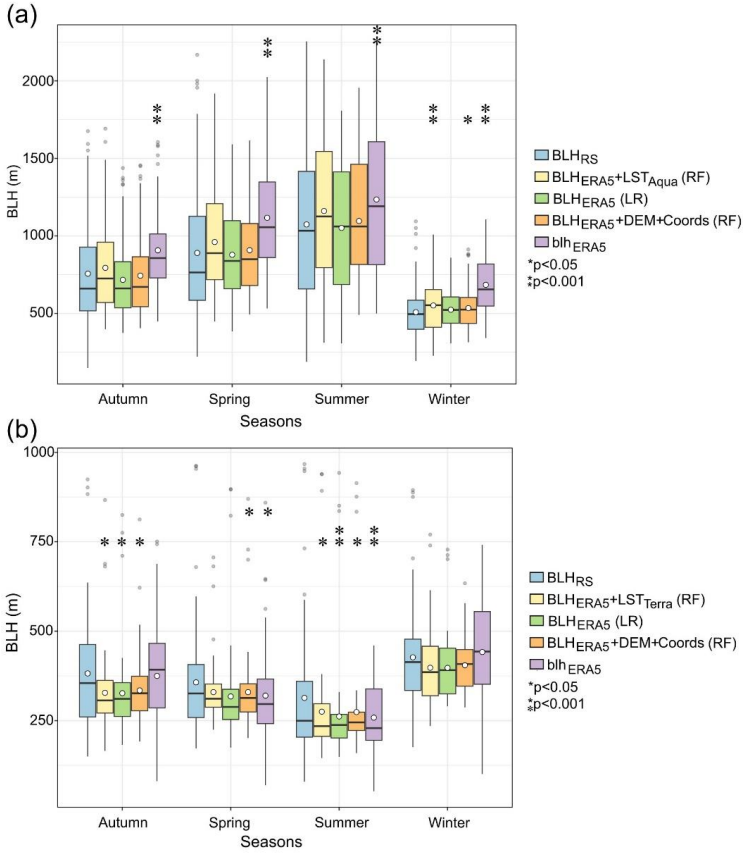

Figure 3 Boxplot of boundary-layer height from observation (BLH_{RS}, 2021-2024 yrs), Copernicus (blh_{ERA5}, 2021-2024 yrs), and from the interpolation models (2010-2020 yrs), divided by seasons. (a) 12:00 UTC and (b) 00:00 UTC. Significant differences with BLH_{RS} values were indicated by *. Other references in Figure 2.

At 12:00 UTC, although the overall pattern appeared similar, significant differences were found between the models and the observed values (Fig. 3a). The interpolated estimates were closest to the observations in autumn, spring, and summer, whereas in winter only the model including BLH_{ERA5} as the unique predictor was not statistically different from the observations (RMSE = 123 m; Table 4). Predictions were more biased during the warmest months (e.g., RMSE ~ 230 m), while in winter and autumn, RMSE values ranged between 123 - 184 m. In addition, as previously observed

https://doi.org/10.5194/egusphere-2026-702
Preprint. Discussion started: 9 March 2026

in the spatial validation, blh_{ERA5} systematically overestimated the observed values across all seasons, with RMSE values ranging from 235 to 346 m (Table 4).

Table 3 Root mean square error (RMSE, metres) between observed values (BLH_{RS}), blh_{ERA5}, and model estimates sorted by climatic season, using an independent dataset (13 stations at 12:00 UTC and 10 stations at 00:00 UTC). Regression models used in the deterministic component are indicated in parentheses: LR = Linear Regression; RF = Random Forest. 'N' indicates the number of stations considered in each season.

UTC	Models	Winter	Spring	Summer	Autumn
12:00	BLH_{ERA5} (LR)	36	187	283	84
	BLH_{ERA5}+DEM+Coords (RF)	40	162	182	154
	BLH_{ERA5}+LST_{Aqua} (RF)	80	164	222	132
	blh_{ERA5}	235	375	466	290
	N	7	8	8	10
00:00	BLH_{ERA5} (RF)	65	34	51	36
	BLH_{ERA5}+DEM+Coords (RF)	68	66	44	36
	BLH_{ERA5}+LST_{Terra} (RF)	77	72	97	36
	blh_{ERA5}	94	45	63	132
	N	6	3	2	9

At 00:00 UTC, the performance of the interpolated models decreased compared with midday. In autumn, although blh_{ERA5} exhibited a higher RMSE than the interpolation models, its mean value was closer to the observations, as shown in Fig. 3b. During summer and winter, all models performed similarly, showing lower accuracy (underestimation) in summer and closer agreement with the observations in winter (Fig. 3b). RMSE values for the interpolation models were similar and, in all cases, lower than those obtained for the Copernicus product (Table 4). Overall, at both times of the day, the BLH_{ERA5} and BLH_{ERA5} + DEM + Coords models achieved equal or better performance in comparison with LST.

To plot the BLH gridded map obtained at each UTC, we selected the BLH_{ERA5} + DEM + Coordinates (RF) configuration for 12:00 UTC and the BLH_{ERA5} (RF) configuration for 00:00 UTC. Although the models achieved similar performance, these combinations yielded the lowest average RMSE in both spatial and temporal validation (Fig. 4).

https://doi.org/10.5194/egusphere-2026-702
Preprint. Discussion started: 9 March 2026

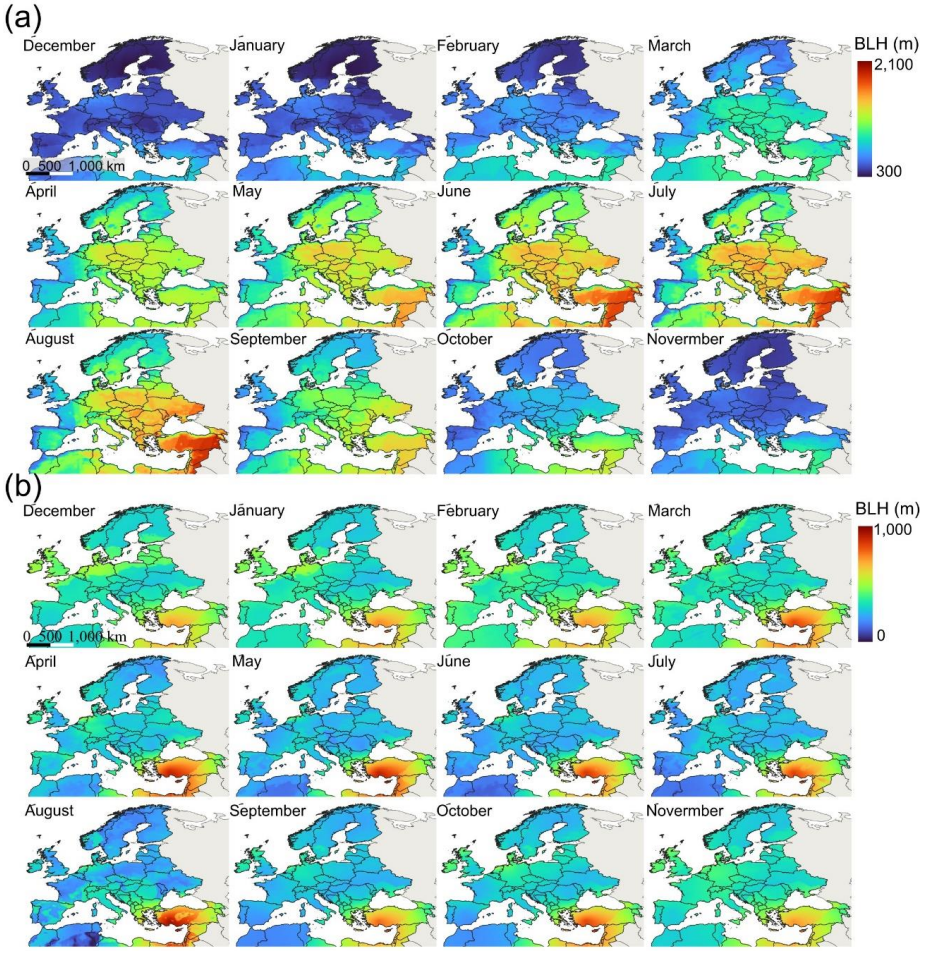

Figure 4 Monthly gridded maps of boundary layer height obtained with Regression Kriging for the study area. a) 12:00 UTC data with BLH_{ERA5} + DEM + Coords (RF) as covariates. b) 00:00 UTC data with BLH_{ERA5} (RF) as covariate.

3.3 Case Study

In this section, the aim was to evaluate the performance of the proposed methodology in predicting BLH values at the regional scale and on a daily temporal resolution.

Germany was selected as the study area based on data availability. From the 2010-2020 dataset, a subset of 15 consecutive days was extracted (allowing for a loss of up to two days per time series), in two contrasting climatic seasons (summer and winter). For 00:00 UTC, only the winter season was available, and with few stations due to the

https://doi.org/10.5194/egusphere-2026-702
Preprint. Discussion started: 9 March 2026

heterogeneity of the working dataset. The details of the dataset obtained for each hour are presented in Table 2B.

Table 4 Root mean square error (RMSE, metres) between observed values (BLH_{RS}; 2021-2024 yrs), model estimates (2010-2020 yrs), and blh_{ERA5} (2021-2024 yrs), sorted by climatic season. Regression models used in the deterministic component are indicated in parentheses: LR = Linear Regression; RF = Random Forest. By season, we had 34 stations at 12:00 UTC and 23 stations at 00:00 UTC.

UTC	Covariate (model)	Winter	Spring	Summer	Autumn
12:00	BLH_{ERA5} (LR)	123	225	244	184
	BLH_{ERA5}+DEM+Coords (RF)	124	223	247	167
	BLH_{ERA5}+LST_{Aqua} (RF)	141	216	256	173
	blh_{ERA5}	235	346	339	273
00:00	BLH_{ERA5} (RF)	117	97	132	117
	BLH_{ERA5}+DEM+Coords (RF)	125	95	123	120
	BLH_{ERA5}+LST_{Terra} (RF)	129	112	131	127
	blh_{ERA5}	202	217	239	207

For each daily period and UTC hour, Regression Kriging was applied using the Random Forest model as the regression component, due to its superior performance compared with Linear Regression (LR) and Gradient Boosting (GB). The covariates used were BLH_{ERA5} + DEM, which showed acceptable performance in both UTC hours and validation procedures.

Meteorological conditions were evaluated for each period at 500 hPa (geopotential height) and 850 hPa (temperature) using data from Wetterzentrale (www.wetterzentrale.de), to assess the coherence of our results. Subsequently, we compared our gridded maps with the reanalysis data by calculating the pixel-wise bias, MAE, and RMSE between blh_{ERA5} and BLH_{pred}, to evaluate the performance of the interpolated values obtained for the period. The main results for each hour and climatic season are detailed below.

3.3.1 12 UTC

3.3.1.1 July 6th to 20th, 2016. Summer (Figure A4)

The meteorological conditions were typical of summer, with isobars around 1000 hPa, warm air, and a stable atmosphere (more pronounced in the South and Centre). Between the 10th and 13th, instability increased (denser air over the north of the country), with a chance of rain and cloudiness. Afterwards, stability returned, accompanied by thermal increase, leading to very warm and dry days. In general, the northern part of the

https://doi.org/10.5194/egusphere-2026-702
Preprint. Discussion started: 9 March 2026

country was more affected by unstable conditions, characterized by cloud cover and rainfall.

In our predicted maps, we observed during the first five days that values above 1,500 m are in the central and southern parts of the region, while in the north, they range from 1,500 to 1,000 m. The days with atmospheric instability are reflected by a decrease in BLH from July 10th to 15th, except on July 11th and 12th. During the remaining days, values tend to fall within the range of 1,400–1,800 m, occasionally dropping 800 m below in the northern area (e.g., on July 16th and 19th).

3.3.1.2 January 4th to 18th, 2012. Winter (Figure A5)

Overall, the conditions were typical of winter, temperatures ranged from -35 to -20°C, characterized by dense cold air, an unstable atmosphere, and a high probability of rain and snow, accompanied by moderate winds. From the 4th to the 5th and the 11th to the 13th of January, the region was affected by a storm with strong winds, snow, and very low temperatures (due to a low-pressure centre north of Germany, over the Atlantic).

In our predicted maps, we observed that on the stormy days with (very) strong winds (4th to 5th and 12th to 13th), BLH values were higher compared to the days with lighter winds under the same cold and snowy conditions.

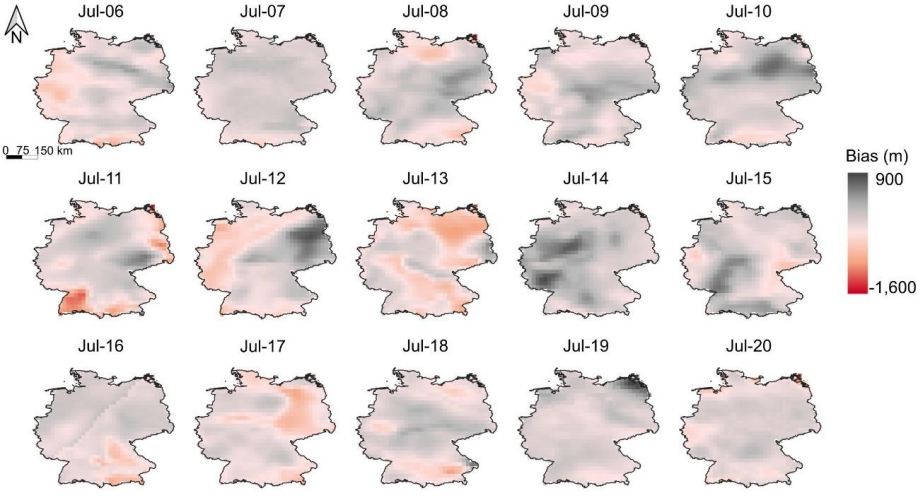

Figure 5 Bias (blh_{ERA5} - $BLH_{pred.}$) of daily gridded maps obtained at 12:00 UTC for the period July 6th to 20th, 2016 (Summer). Reddish areas indicated that pixel values of $BLH_{pred} > blh_{ERA5}$; grey areas the opposite.

https://doi.org/10.5194/egusphere-2026-702
Preprint. Discussion started: 9 March 2026

3.3.1.3 Reanalysis comparison

When the predicted values were compared with the reanalysis, fifteen daily maps were produced, showing two predominant colours: grey pixels indicating blh_{ERA5} > BLH_{pred}, and red areas indicating BLH_{pred} > blh_{ERA5} (Fig. 5).

In summer, the mean bias (± std) for the time series was −90.8 ± 121 m, while the RMSE was 279 ± 83 m and the MAE was 220 ± 72 m. Extreme bias values were rare and were mostly observed in the southern part of the study region (e.g., July 11th, bias ~ 1,500 m). In the northern and central regions, blh_{ERA5} tended to exhibit higher values than those predicted by the model. However, no clear spatial pattern or systematic tendency was identified.

Considering the meteorological conditions during the analysed period, the days from the 10th to the 13th of July were characterised by cloud cover and a high probability of rainfall, conditions typically associated with lower BLH values. During this period, the reanalysis values were higher than those derived from the interpolation model (grey-shaded areas) on July 10th and 11th, whereas on July 12th and 13th the pattern was slightly reversed. In contrast, under more stable conditions, such as those observed from July 16th to the 20th, the predicted values tended to exceed those from blh_{ERA5} in certain regions by more than 500 m.

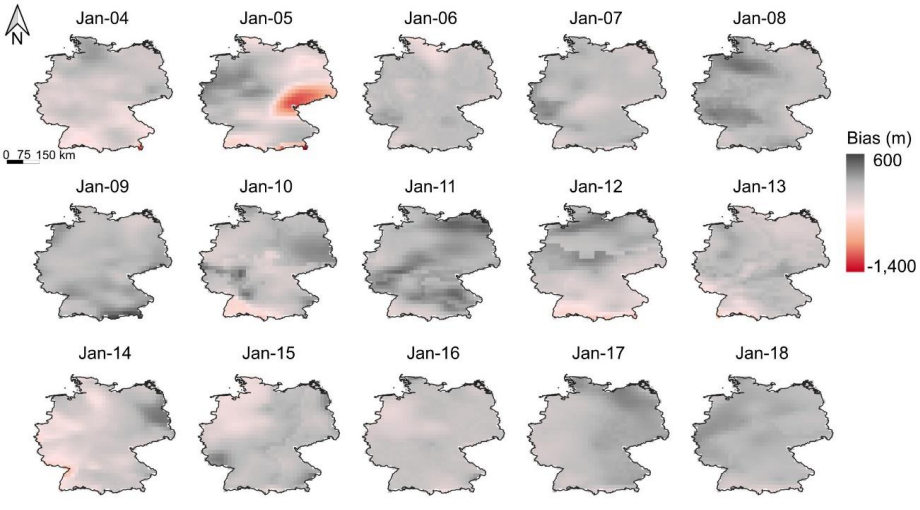

Figure 6 Bias (blh_{ERA5} - $BLH_{pred.}$) of daily gridded maps obtained at 12:00 UTC for the period January 4th to 18th, 2012 (Winter). Reddish areas indicated that pixel values of BLH_{pred} > blh_{ERA5}; grey areas the opposite.

https://doi.org/10.5194/egusphere-2026-702
Preprint. Discussion started: 9 March 2026

In winter, differences between the models were less pronounced than in summer. The parameters between models for the time series were bias = 20 ± 87 m, RMSE = 161 ± 69 m, and MAE = 126 ± 51. In general, blh_{ERA5} exhibited higher values than those predicted by the model (Fig. 6). The largest bias values occurred on 5 January in the south-eastern sector of the study region (one pixel). During the winter storm events of January 4th to 5th and 11th to 13th, the predictive model estimated a shallower BLH than ERA5 by approximately 300 m, except for a small area in the central-eastern part of the region on January 5th.

For both seasons, the extreme differences between the models were mainly due to higher values estimated by the interpolation model in the marginal areas of the study region.

3.3.2 00 UTC

3.3.2.1 January 1st to 15th, 2013. Winter (Figure A6)

For the first five days, no data were available. From the 6th onward, low temperatures typical of the area in winter were recorded (-30 to -25°C, not as extreme as the same period the previous year), with slight instability that gradually increased until the 11th and 12th, when there was a chance of rain/snow, though the storms were weaker than in 2012. Afterwards, the weather became more stable, cold, and dry.

In our predicted maps, for the ten days for which meteorological information was available, the weather conditions were homogeneous (with no severe storms), and the values predicted by the model were also quite similar each day, indicating a very shallow boundary layer. An exception occurred on January 13th and 14th, when a small area in the northeast exhibited unusually high values. Overall, the results were better than expected, considering the low number of stations (N = 8) at UTC.

3.3.2.2 Reanalysis comparison

When the predicted values were compared with the reanalysis, no large differences with ERA5 were found. The mean parameter values were bias = -46 ± 87 m, RMSE = 202 ± 59 m, and MAE = 159 ± 48 m. These values indicate that, although the predictive model tends to produce higher BLH values than ERA5, the differences between them are on the order of 200 m and remain consistent throughout the time series (e.g.,

https://doi.org/10.5194/egusphere-2026-702
Preprint. Discussion started: 9 March 2026

standard deviation < 100 m). The predicted values were higher in the south, while those from ERA5 were higher in the central and northern areas. No major differences were observed except in the north-east on January 13th, where the most extreme values occurred.

Regarding the meteorological conditions during the study period, during the period of marked atmospheric instability (January 6th to 13th), there was a slight tendency for blh_{ERA5} to produce a deeper boundary layer (approximately 300 m) than the interpolated method (grey-shaded areas). This tendency persisted until the end of the time series.

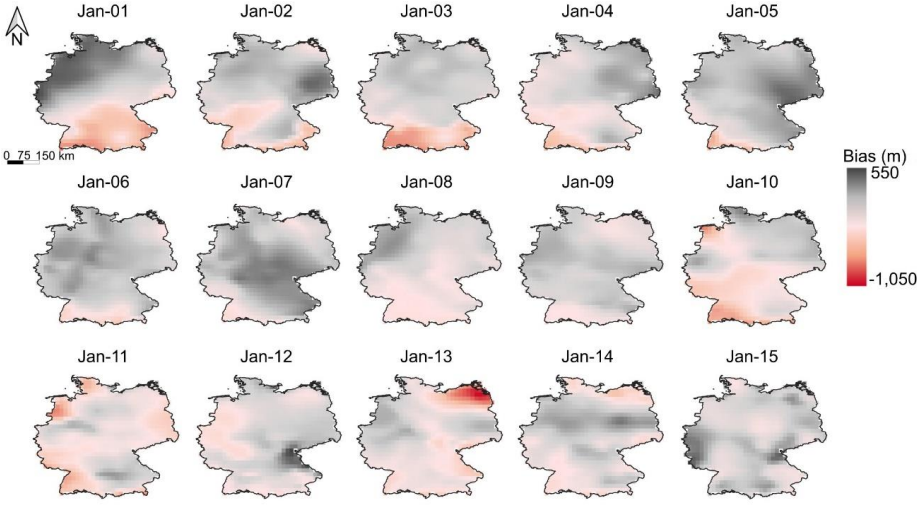

Figure 7 Bias (blh_{ERA5} - $BLH_{pred.}$) of daily gridded maps obtained at 00:00 UTC for the period January 1st to 15th, 2013 (Winter). Reddish areas indicated that pixel values of $BLH_{pred} > blh_{ERA5}$; grey areas the opposite.

4. Discussion

In the present study, gridded maps (25 x 25 km2 and monthly means) of the planetary boundary layer were produced by combining different data sources using the regression kriging method. Our main finding is the higher spatio-temporal accuracy achieved in comparison with another widely used and validated product, namely the ERA5 reanalysis.

The distinct stages in the dynamics of the planetary boundary layer were reflected in the differences in model performance between midday (12:00 UTC, convective

https://doi.org/10.5194/egusphere-2026-702
Preprint. Discussion started: 9 March 2026

boundary layer) and midnight (00:00 UTC, stable boundary layer). The results at midday showed better performance than those obtained at night. In both cases, however, combining reanalysis, topographic (DEM) and LST covariates, and Linear Regression (12:00 UTC) and Random Forest (12:00 and 00:00 UTC) provided the best representation of the observed values, sometimes outperforming the ERA5 reanalysis.

Moreover, we applied a specific case study at a higher temporal resolution, which revealed a strong coherence between the interpolated model and the prevailing weather conditions. Differences with ERA5 were on average below 200 m, demonstrating the usefulness of this approach for mesoscale analyses and its potential applicability in climate modelling. The main results and future steps are discussed below.

4.1 Interpolation method

Recently, several studies have employed machine learning models to estimate or predict the planetary boundary layer. For instance, Ayazpour et al., (2023) produced a gridded map across the USA using eXtreme Gradient Boosting, improving the estimated BLH values in some cases (RMSE > 200 m) compared to reanalysis BLH data (e.g., ERA5, MERRA, and NARR). In a global-scale study, Guo et al., (2024) estimated the differences (bias) between BLH obtained from radiosondes and ERA5 using Random Forest regression alongside climatic and physical variables. They obtained a corrected BLH value which, when compared with radiosonde BLH, yielded a mean absolute bias of 168 m. Finally, Zhang et al., (2025), at an atmospheric observatory in Oklahoma (USA), modelled BLH values at 10-minute intervals using three ML algorithms; The best-performing model achieved an RMSE of approximately 110 m stable and 240 m for unstable BL. Notwithstanding the methodological differences, sample sizes, and study areas, our work has yielded similar results in terms of error parameters (Tables 1, 2, 3, and 4), thereby validating the methodology applied in the present study.

We opted for regression kriging rather than ML tools for prediction because, in RK, once the deterministic component of variation has been estimated, the residuals can be interpolated using kriging and added to the estimated trend. Therefore, if there is a strong correlation between the target variable and the covariates, the residuals are small or close to zero, and the prediction relies on the regression model. Conversely, if there is no strong correlation between the variables, the prediction depends on the spatial autocorrelation of the residuals (Hengl et al., 2007). This reinforces the predictive

https://doi.org/10.5194/egusphere-2026-702
Preprint. Discussion started: 9 March 2026

capability of the proposed approach. As noted by Argañaraz et al., (2025), Universal Kriging (similar to RK) outperformed Gradient Boosting Forest and Radial Basis Function methods in predicting climatic variables, a result attributed to the influence of spatial autocorrelation. This approach, which combines two concepts, has been successfully applied in other studies involving the spatial interpolation of climatic variables (Krähenmann et al., 2018; Asadi Oskouei et al., 2022).

4.2 Relevance of covariates

No significant differences were found when comparing the RMSEr results across the different combinations of covariates. This may be related to several factors, such as the low correlation (< 0.75) between the variables used and BLH_{RS}. However, as shown in Figure 3A, the monthly standard deviations overlap considerably. In both hours, the combination of the land surface temperature (LST) and DEM with BLH_{ERA5} values provides the most favourable configuration for predicting planetary boundary layer data. Nevertheless, this difference is overshadowed by the large dispersion of the results. This data spread could be related to the sampling and structural uncertainties associated with the method, which can amount to several hundred metres, up to 1 km (Seidel et al., 2010). This introduces an intrinsic variability in the BLH_{RS} data (used as targets), which is subsequently reflected in our results.

The relevance of BLH_{ERA5} and DEM is not unexpected. In the case of BLH_{ERA5}, it corresponds to the target variable, derived from ECMWF data assimilation, which has previously been reported to show good accuracy when compared with radiosonde observations (Guo et al., 2021; Li et al., 2023; Xu et al., 2023). Moreover, it has previously been reported as a highly relevant covariate for predicting observed BLH values (Ayazpour et al., 2023). However, it was not sufficient on its own to provide the best estimation of the observed values. This outcome may be associated with several factors, such as differences in the calculation of the Richardson number, or the coarse vertical resolution compared with radiosondes, and other possible factors have been previously discussed in other works (Seidel et al., 2010; Guo et al., 2021; Madonna et al., 2021; Dias-Júnior et al., 2022; Sinclair et al., 2022; Slättberg et al., 2022; Xu et al., 2023; Guo et al., 2024; etc.).

https://doi.org/10.5194/egusphere-2026-702
Preprint. Discussion started: 9 March 2026

Several studies have reported reduced performance of the ERA5 reanalysis product in regions with complex topography, e.g., for climatic variables (Cavalleri et al., 2024; Crespi et al., 2024) and boundary layer height (Guo et al., 2021, 2024). This may explain why including DEM could improve the prediction of observed values. Terrain elevation serves as an indirect indicator of topographic variation, such as valleys, plateaus, and slopes, which influences the dynamics of air mass flows. These flows interact directly with the BLH and vary between daytime and nighttime conditions. Such variation reduces the accuracy of measurement instruments compared with flat terrain (De Wekker and Kossmann 2015), introducing a source of uncertainty that can be diminished by incorporating the altitude values of each pixel.

The use of geographical coordinates (Coords) as covariates produces acceptable results in combination with DEM and LST, which is related to the relevant influences of geographic position over the development of the planetary boundary layer. For example, latitude is associated with the amount of solar radiation reaching the Earth's surface. As we move away from the equator, the incoming solar radiation per unit area decreases (Stull, 1988), explaining the negative correlations with BLH_{RS} (Table B1). In turn, longitude is directly related to solar time. Stations located on the western side of the study area (~UTC +1) receive a different time exposure of sunlight than those on the eastern edge (~UTC +3) at the same UTC (Seidel et al., 2012; Guo et al., 2021).

Although the LST showed a moderate ability to predict the observed values, when considered alongside air temperature and wind speed, these climatic variables were far from reaching the level of relevance we had expected. According to the literature, an increase in surface temperature or wind speed is generally associated with greater development of the BLH (Seidel et al., 2012; Guo et al., 2016; Li et al., 2023). However, in other studies, wind speed (Ayazpour et al., 2023; Zhang et al., 2025) and air temperature (Zhang et al., 2025) have been excluded from BLH modelling due to their low relevance in regression-based models.

It is worth mentioning that several limitations in the covariate datasets used may have directly influenced our results. a) *The available LST values*. Only clear-sky days were considered, which may have led to higher PBL development, since there is a direct relationship between clear-sky, without clouds, conditions and PBL growth, and consequently its height (Quan et al., 2013; Guo et al., 2016). Moreover, this restriction

https://doi.org/10.5194/egusphere-2026-702
Preprint. Discussion started: 9 March 2026

reduced the number of daily values per station. This influenced the monthly means used in the interpolation and ultimately affected the realistic representation of the PBL. b) *Station density*. The E-OBS variables (TX, TG, and FG) were represented by a relatively low station density, mainly due to spatial cover limitations. It is well known that low spatial density directly affects the accuracy of the interpolation methods (Krähenmann et al., 2018; Argañaraz et al., 2025). c) *Data inhomogeneity*. Although the E-OBS dataset has been regularly updated since 1950, it still presents uneven station coverage across Europe. Variations in data density over time, together with inconsistencies in the observation records, may influence the representation of long-term climate variability in the gridded datasets (Crespi et al., 2024). d) *Coarse temporal resolution*. Another important aspect concerns the daily and effectively 24-hour temporal resolution of the E-OBS variables (TG, TX, and FG). This inevitably introduces bias, as the same gridded values must be used for both synoptic hours. Consequently, these inputs resemble broad daily averages rather than precise time-specific measurements.

4.3 Seasonal and daily performance

The planetary boundary layer exhibits a pronounced diurnal cycle, with its height varying from only a few tens of metres at night to over one kilometre during the day, and with different levels of uncertainty associated with these measurements (Seidel et al., 2012; Guo et al., 2021). Despite the limitations related to the number of available stations, our results were consistent with previously reported patterns for the European region, showing higher BLH values in summer during the day, and in winter during the night (Fig.2, 3, and 4) (Seidel et al., 2012). Moreover, for both validation approaches, we found higher RMSE values during the warm seasons than during the cold seasons, with this contrast being more pronounced during daytime than at night. This finding is consistent with Guo et al., (2021), who reported a similar seasonal pattern at the global scale, based on bias values between observations and four different reanalysis products.

Spatial validation revealed that the results obtained at night were more heterogeneous than those obtained during the day. This may be related to the smaller number of stations available for interpolation at 00:00 UTC, which increases uncertainty in areas with low station density (Krähenmann et al., 2018). Moreover, a reduced number of samples inevitably leads to an increase in the standard deviation.

https://doi.org/10.5194/egusphere-2026-702
Preprint. Discussion started: 9 March 2026

The poor cross-validation performance at night may be attributed to the weak or non-existent relationship between climatic variables and BLH during nighttime (Seibert et al., 2010; Zhang et al., 2020). However, despite RMSEr values being close to or higher than 1, the interpolation models still performed better than the blh_{ERA5} data available for the same locations (e.g., in winter and autumn, Table 3; Fig 2b). Furthermore, the substantial difference in BLH between day and night, typically >1 km during the day and <0.5 km at night, further increases the uncertainty values at night, which may be due to the limited vertical resolution of the available instruments (Seibert et al., 2010; Seidel et al., 2012). The poor performance at night is also reflected in the gridded maps, which show more homogeneous monthly patterns at night (Fig. 4b), whereas during the day (Fig. 4a), clear seasonal variability is evident among the maps, a behaviour that has previously been described as characteristic of the planetary boundary layer.

During temporal validation at 12:00 UTC, significant differences were detected among the interpolation models and reanalysis, being the interpolation models more accurately than ERA5 values. It is important to note that blh_{ERA5} values share the same temporal scale as the observation (BLH_{RS}) data. Consequently, this highlighted the performance of the interpolation models, which were developed using data from the 2010-2020 period. This finding was contrasted at night, where the blh_{ERA5} were similar to the observations in the coldest seasons, whereas the interpolation models lost precision in summer and winter (Fig. 3b). However, the models exhibited lower RMSE values than blh_{ERA5}. Although this may seem contradictory, it can be explained by the higher dispersion of blh_{ERA5} values compared with the models, as reflected by the elongated boxplots in Fig. 3b. This highlights a limitation in predicting BLH at night, as previously observed in the spatial validation. This limitation is not exclusive to our interpolation models; previously, several authors have reported it for reanalysis products (Seidel et al., 2012; Sinclair et al., 2022; Xu et al., 2023), BLH estimates derived from lidar observations (Zhang et al., 2025), and radiosonde measurements (Gu et al., 2020).

Our results highlight the potential of simple tools such as interpolation to generate gridded maps that provide improved approximations of the stable boundary layer (SBL) at new areas and CBL in known and new areas, using widely available variables such as the DEM and blh_{ERA5}.

https://doi.org/10.5194/egusphere-2026-702
Preprint. Discussion started: 9 March 2026

4.4 Study case performances

We applied the proposed methodology to a mesoscale case study with a daily temporal resolution. Our results revealed a clear relationship between daily meteorological variations and BLH values in the time series. For instance, areas with higher probabilities of precipitation and cloud cover exhibited lower BLH values compared with regions showing greater atmospheric stability and clear-sky conditions (see Figure A4, July 11th to 15th). This pattern is associated with increased relative humidity and reduced incoming solar radiation, which in turn decreases the amount of sensible heat flux available for boundary-layer development (Dias Júnior et al., 2022; Li et al., 2023). Moreover, another consistent finding concerned the effect of strong winds and atmospheric instability in deepening the PBL (Guo et al., 2016; Sinclair et al., 2022), as observed during the days of severe storms (Figure A5, January 12th, 4th to 5th and 12th to 13th).

In addition to being consistent with the prevailing meteorological conditions, the predicted values were also compared with ERA5 estimates. During daytime, predicted BLH values alternated between being lower and higher than ERA5 in summer, whereas in winter, values were consistently lower than ERA5 (Figs. 5 and 6). This behaviour is consistent with our previous results, where at 12:00 UTC during summer, blh_{ERA5} and model estimates were broadly comparable, while in winter the reanalysis systematically exhibited higher values than the models.

Numerous comparative studies in the literature report that ERA5 tends to underestimate radiosonde-derived BLH during daytime (Guo et al., 2016, 2021, 2024; Sinclair et al., 2022; Dias Júnior et al., 2022; Slättberg et al., 2022). Considering that in summer, the mean bias was -90 ± 121 m in favour of the interpolation model. The predicted values exceeded those of the reanalysis during stormy periods and under stable atmospheric conditions. These results suggest that the interpolated estimates may represent the observed BLH more accurately. However, during winter, the scheme changes, and our model predicts a shallow BLH with respect to reanalysis. This could be related to the difficulties in resolving a BLH of a few hundred meters by ERA5, which is the main source of our model, additionally to the few numbers of stations available.

With one exception, the predicted values at night were lower than those from ERA5 across the entire study region (Fig. 7). According to the literature, ERA5 tends to

https://doi.org/10.5194/egusphere-2026-702
Preprint. Discussion started: 9 March 2026

underestimate radiosonde-derived BLH during nighttime, for example, in central Amazonia (Dias Júnior et al., 2022) and over the Tibetan Plateau (Slättberg et al., 2022). However, other studies have reported an overestimation of ERA5 relative to radiosonde measurements, such as at the global scale (Seidel et al., 2012), in Hyytiälä, Finland (Sinclair et al., 2022), and over China, where Xu et al. (2023) found that the reanalysis overestimated mean stable boundary layer height, with values ranging from 399.3 to 1645.3 m. Moreover, these discrepancies are more pronounced during the warm season than during colder periods (Guo et al., 2021, 2024). Considering this contrasting evidence, it is difficult to determine whether our predictions perform better or worse than the reanalysis.

Considering the inherent challenges associated with the methods and instruments used to estimate the stable boundary layer (SBL), as well as the limitations specific to our study, such as the reduced number of stations at 00:00 UTC, limited coverage in the southern part of the region, and edge effects commonly associated with interpolation procedures; These and other factors may have contributed to the observed discrepancies. Consequently, it is not possible to assert whether our estimates are better or worse than those provided by ERA5.

Therefore, based on this comparison alone, we cannot confidently state whether our values are close to observed values or not, especially at night. Further studies are required to confirm or refute these findings.

5. Conclusion

In this study, we implemented a classic technique, such as regression kriging, to obtain gridded maps of the planetary boundary layer height at two synoptic hours, integrating multiple data sources. The approach, despite its limitations, yielded good spatial and temporal accuracy compared with the ERA5 reanalysis.

The combination of reanalysis and topographic covariates provided the most accurate estimates. Moreover, reflecting the inherent complexity of the boundary layer, the machine-learning methods used to estimate spatial correlation consistently outperformed linear regression.

Model performance differed between midday (convective boundary layer) and midnight (stable boundary layer). In the spatial validation, both during the day and at night, the interpolation models provided a closer approximation to the observed values

https://doi.org/10.5194/egusphere-2026-702
Preprint. Discussion started: 9 March 2026

than ERA5. During the temporal validation, the interpolation models were more accurate during daytime than ERA5 and exhibited reduced accuracy at night. Overall, the main limitations were observed during nighttime.

A mesoscale case study demonstrated the method's potential for application in climate modelling. The promising results obtained compared with the reanalysis encourage testing the efficacy of incorporating these data into mesoscale model simulations. Considering that our analysis is based on a limited number of stations, we strongly believe that the performance of this interpolation method could be substantially improved with a denser coverage of meteorological stations, potentially yielding better results than those obtained here and enhancing those from currently available reanalysis products.

Appendix A

Figure A1: Root mean square error (RMSE) for each temperature variable comparison at each time by month. Although the differences were not statistically significant in all cases, TX and LST_{Aqua} showed lower error values at 12:00 UTC (a), while TG and LST_{Terra} performed better at 00:00 UTC (b).

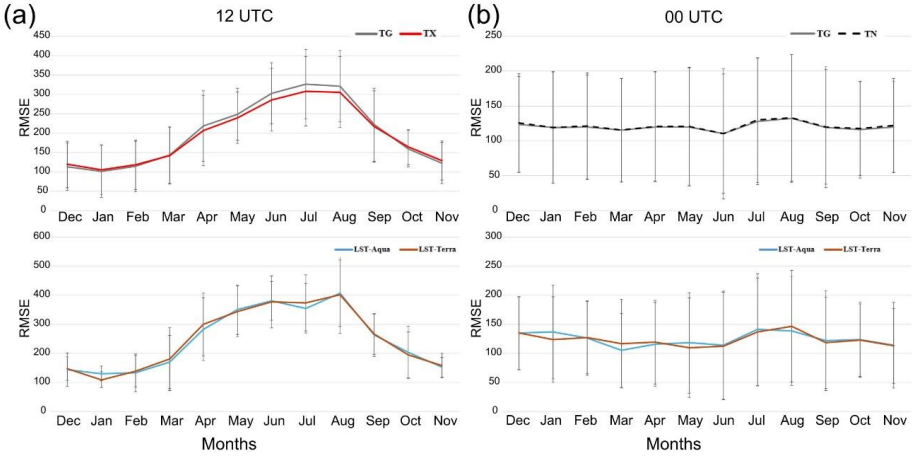

https://doi.org/10.5194/egusphere-2026-702
Preprint. Discussion started: 9 March 2026

Figure A2: Spatial distribution of stations used for spatial validation. References are provided in the figure

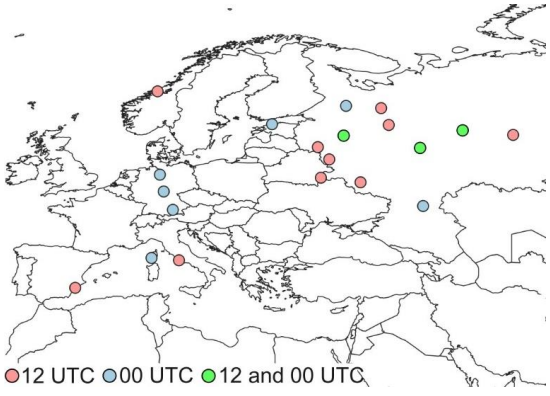

865

https://doi.org/10.5194/egusphere-2026-702
Preprint. Discussion started: 9 March 2026

Figure A3: Monthly RMSEr obtained by cross-validation (2010-2020 period). The model covariates combination with the better performance were plotted (mean±std). (a) 12:00 UTC (b) 00:00 UTC. The lines are colour-coded according to the legend behind each UTC graph.

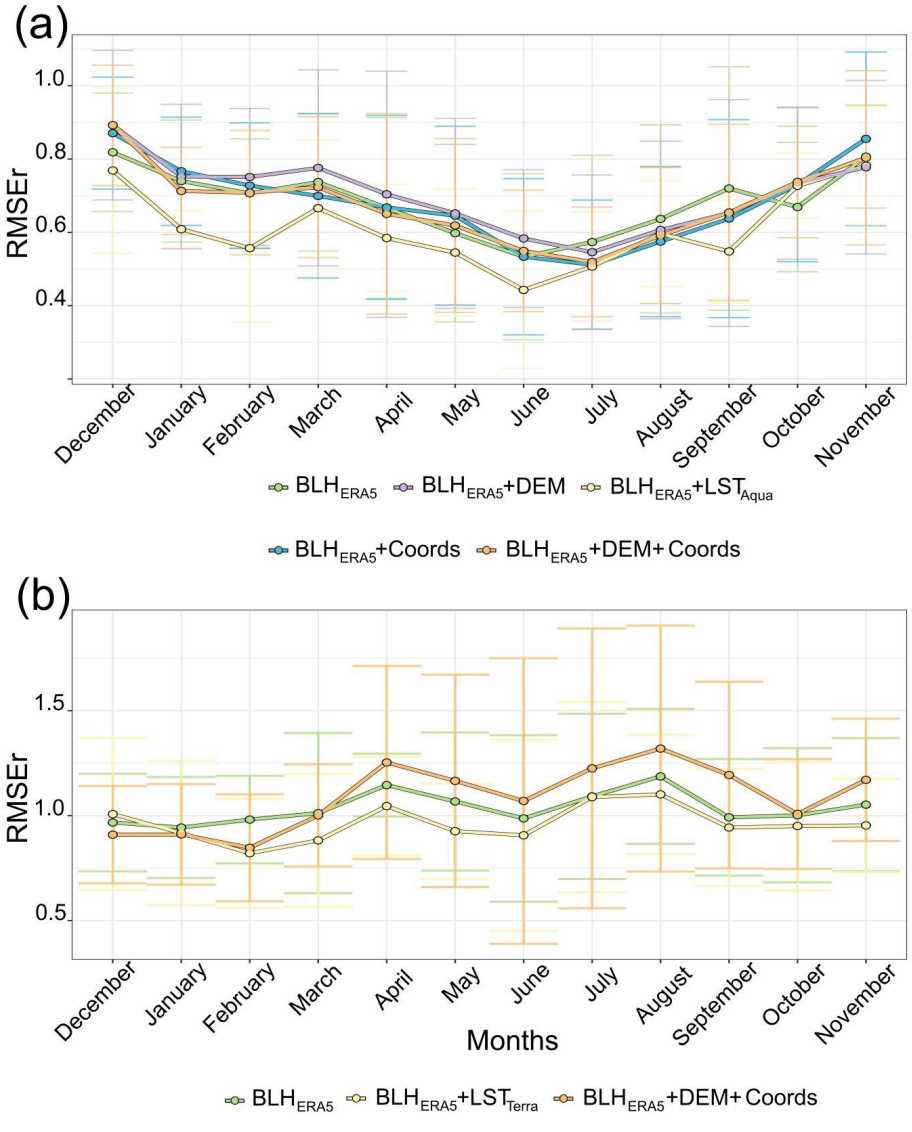

https://doi.org/10.5194/egusphere-2026-702
Preprint. Discussion started: 9 March 2026

Figure A4: Daily gridded maps obtained at 12:00 UTC for the period July 6th to 20th, 2016 (Summer). The spatial distribution of training stations and boundary-layer height references are shown at the bottom.

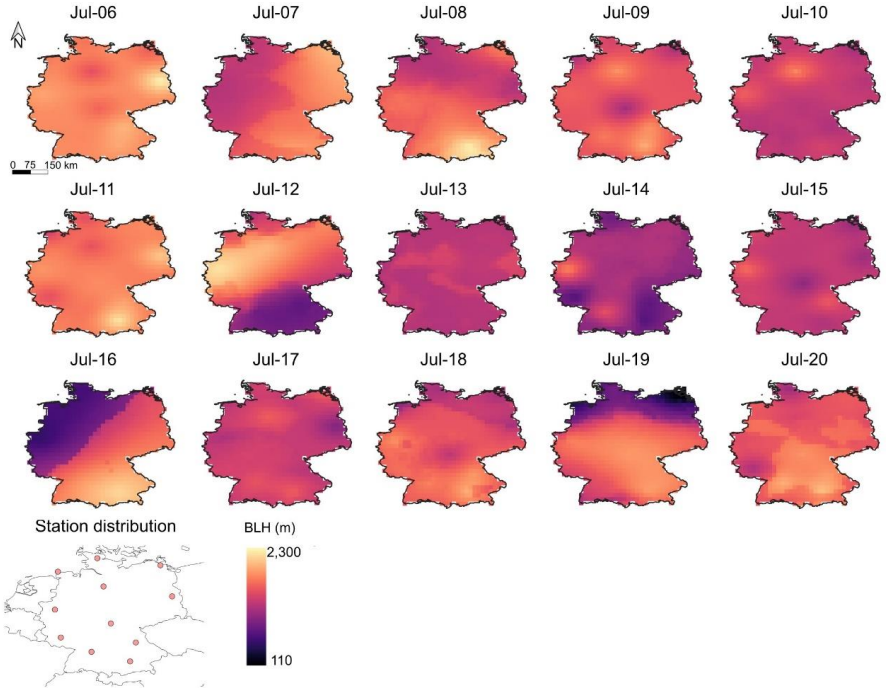

https://doi.org/10.5194/egusphere-2026-702
Preprint. Discussion started: 9 March 2026

Figure A5: Daily gridded maps obtained at 12:00 UTC for the period January 4th to 18th, 2012 (Winter). The spatial distribution of training stations, the number of days per station, and the boundary-layer height references are shown at the bottom

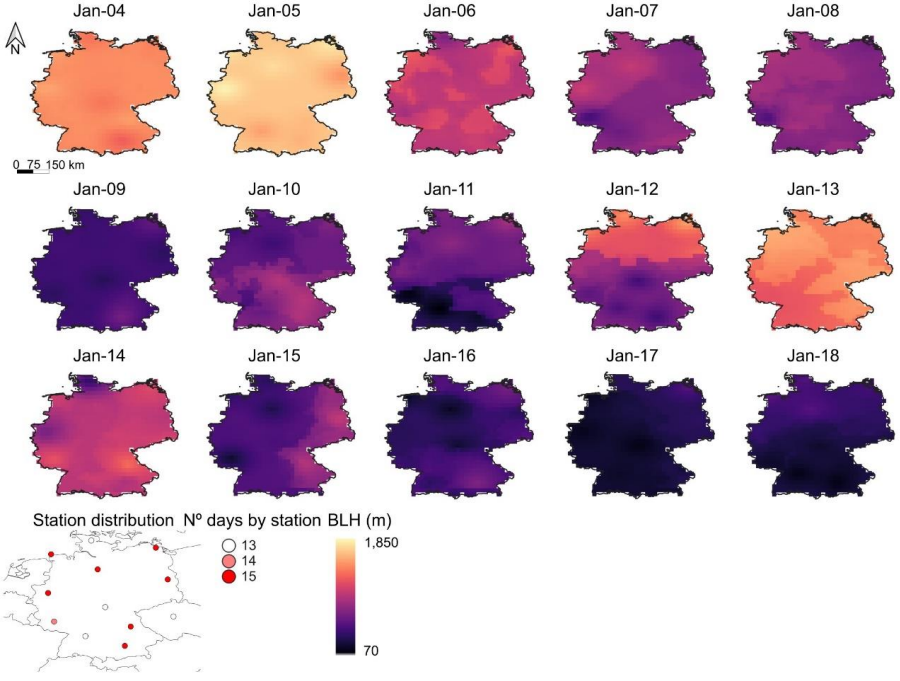

https://doi.org/10.5194/egusphere-2026-702
Preprint. Discussion started: 9 March 2026

Figure A6: Daily gridded maps obtained at 00 UTC for the period January 1st to 15th, 2013. The spatial distribution of training stations, the number of days per station, and the boundary-layer height references are shown at the bottom.

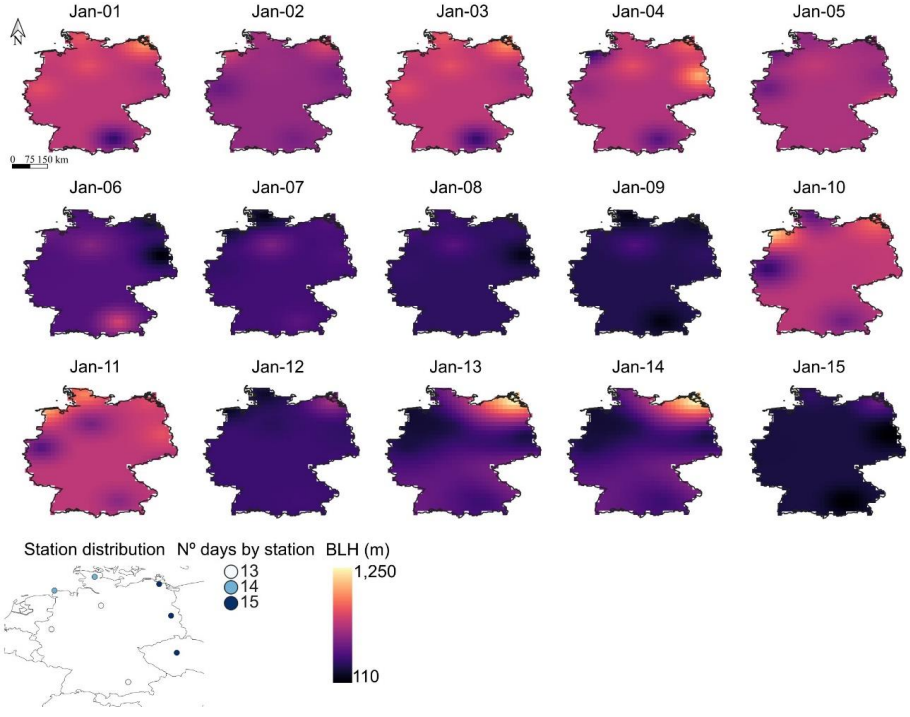

https://doi.org/10.5194/egusphere-2026-702
Preprint. Discussion started: 9 March 2026

Appendix B

Table B1: Environmental variables and the mean correlation value, Pearson (r) and Spearman (ρ), between stations' monthly mean of observed boundary layer height (BLH_{RS}) and covariates.

UTC	Source	Variable	Nº Stations	Nº Daily data	r / ρ
12	Radiosonde	BLH_{RS}	44	120829	-
	ERA5	BLH_{ERA5}	44	120829	0.83 / 0.80
	Land surface temperature (MODIS)	LST_{Aqua}	43	46433	0.65 / 0.63
	Maximum air temperature (E-OBS)	TX	36	100520	0.55 / 0.54
	Mean daily wind speed (E-OBS)	FG	24	66482	-0.23 / -0.22
	Geographic location	Latitude	44	-	-0.12 / -0.10
	Geographic location	Longitude	44	-	0.51 / 0.54
	Copernicus DEM	DEM	44	-	0.21 / 0.41
00	Radiosonde	BLH_{RS}	39	103402	-
	ERA5	BLH_{ERA5}	39	103402	0.80 / 0.78
	Land surface temperature (MODIS)	LST_{Terra}	39	44178	-0.64 / -0.65
	Mean daily air temperature (E-OBS)	TG	33	86715	-0.74 / -0.74
	Mean daily wind speed (E-OBS)	FG	25	63086	0.72 / 0.68
	Geographic location	Latitude	39	-	-0.16 / 0.06
	Geographic location	Longitude	39	-	-0.17 / -0.37
	Copernicus DEM	DEM	39	-	0.52 / -0.04

https://doi.org/10.5194/egusphere-2026-702
Preprint. Discussion started: 9 March 2026

Table B2: Details of the datasets used in the case study.

UTC	Time period	N° stations	N° days
12:00	July 6th to 20th, 2016	11	165
	January 04th to 18th, 2012	12	171
00:00	January 1st to 15th, 2013	8	112

900

https://doi.org/10.5194/egusphere-2026-702
Preprint. Discussion started: 9 March 2026

Acknowledgement

We acknowledge the E-OBS dataset from the Copernicus Climate Change Service (C3S, https://surfobs.climate.copernicus.eu) and the data providers in the ECA&D project (https://www.ecad.eu). Google Earth Engine platform for the data, in addition to radiosonde measurements providers, as in Salcedo-Bosch et al. (2025). We acknowledge the Python developers of packages "PyKrige" and "statsmodels".

Funding statement

This research was supported by the National Recovery and Resilience Plan (NRRP), Mission 4, Component 2, Investment 1.1, funded by the European Union - NextGenerationEU – Projects "PBLhsat" CUP P20224AT3 W, "HPC_BIG_DATA_QUANTUM" - E13C22001000006, "VITALITY" - E13C22001060006 - ECS00000041.

Author contributions

CIA: Data curation; Formal analysis; Methodology; Visualization; Writing - original draft; Writing - review and editing. ASB: Data curation, Writing - review and editing. SL: Conceptualization, Writing - review and editing; Funding. GC: Conceptualization; methodology; Writing - review and editing; Supervision; Funding.

Competing interest

The author Simone Lolli is member of the editorial board of journal Atmospheric Measurement Techniques.

References

Argañaraz, C. I., Salcedo-Bosch, A., Lolli, S. & Curci, G. (2025). Building a high-resolution climate gridded dataset in complex terrain: validating different methods in Abruzzo region in Italy. *International Journal of Climatology*, 0:e70153. https://doi.org/10.1002/joc.70153

Asadi Oskouei, E., Delsouz Khaki, B., Kouzegaran, S., Navidi, M. N., Haghighatd, M., Davatgar, N., & Lopez-Baeza, E. (2022). Mapping Climate Zones of Iran Using Hybrid Interpolation Methods. *Remote Sensing*, 14(11), 2632. https://doi.org/10.3390/rs14112632

Ayazpour, Z., Tao, T., Li, D., Scarino, A.J., Kuehn R.E., Sun, K. (2023). Estimates of the spatially complete, observational-data-driven planetary boundary layer height over the contiguous United States. *Atmospheric Measurement Techniques*, 16, 563-580. https://doi.org/10.5194/amt-16-563-2023

Cavalleri, F., Viterbo, F., Brunetti, M. et al., (2024). Inter-Comparison and Validation of High-Resolution Surface Air Temperature Reanalysis Fields Over Italy. *International Journal of Climatology*, 44, 2681-2700. https://doi.org/10.1002/joc.8475.

https://doi.org/10.5194/egusphere-2026-702
Preprint. Discussion started: 9 March 2026

Chen, X., Yang, T., Wang, Z., Wang, F. & Wang, H. (2023). An ensemble method for improving the estimation of planetary boundary layer height from radiosonde data. *Atmospheric Measurement Techniques*, 16, 4289-4302. https://doi.org/10.5194/amt-16-4289-2023

Cornes, R., van der Schrier, G., van den Besselaar, E. J. M. & Jones, P. D. (2018). An ensemble version of the E-OBS temperature and precipitation datasets. *Journal of Geophysical Research: Atmospheres*, 123, 9391-9409. https://doi.org/10.1029/2017JD028200

Crespi, A., Napoli, A., Galassi, G., Lazzeri, M., Parodi, A., Zardi, D. & Pittore, M. (2024). Leveraging observations and model reanalyses to support regional climate change adaptation activities: An integrated assessment for the Marche Region (Central Italy). *Climate Services*, 36, 100512. https://doi.org/10.1016/j.cliser.2024.100512

De Wekker, S. F. J. & Kossmann, M. (2015). Convective boundary layer heights over mountainous terrain — a review of concepts. *Frontiers in Earth Science*, 3, 77. https://doi.org/10.3389/feart.2015.00077

Dias-Júnior, C. Q., Carneiro, R. G., Fisch, G., D'Oliveira, F. A. F., Sörgel, M., Botía, S., Machado, L. A. T., Wolff, S., Santos, R. M. N. d. & Pöhlker, C. (2022). Intercomparison of planetary boundary layer heights using remote sensing retrievals and ERA5 reanalysis over central Amazonia. *Remote Sensing*, 14, 4561. https://doi.org/10.3390/rs14184561

Gu, J., Zhang, Y. H., Yang, N., & Wang, R. (2020). Diurnal variability of the planetary boundary layer height estimated from radiosonde data. *Earth and Planetary Physics*, *4*(5), 479-492. http://doi.org/10.26464/epp2020042

Guo, J., Miao, Y., Zhang, Y., Liu, H., Li, Z., Zhang, W., He, J., Lou, M., Yan, Y., Bian, L. & Zhai, P. (2016). The climatology of planetary boundary layer height in China derived from radiosonde and reanalysis data. *Atmospheric Chemistry and Physics*, 16, 13309-13319. https://doi.org/10.5194/acp-16-13309-2016

Guo, J., Li, Y., Cohen, J. B., Li, J., Chen, D., Xu, H., Liu, L., Yin, J., Hu, K. & Zhai, P. (2019). Shift in the temporal trend of boundary layer height in China using long-term (1979-2016) radiosonde data. *Geophysical Research Letters*, 46, 6080-6089. https://doi.org/10.1029/2019GL082666

Guo, J., Zhang, J., Yang, K., Li, H., Zhang, S., Huang, K., Lv, Y., Shao, J., Yu, T., Tong, B., Li, J., Su, T., Yim, S. H. L., Stoffelen, A., Zhai, P. & Xu, X. (2021). Investigation of near-global daytime boundary layer height using high-resolution radiosondes: first results and comparison with ERA5, MERRA-2, JRA-55, and NCEP-2 reanalyses. *Atmospheric Chemistry and Physics*, 21, 17079-17097. https://doi.org/10.5194/acp-21-17079-2021

Guo, J., Zhang, J., Shao, J., Chen, T., Bai, K., Sun, Y., Li, N., Wu, J., Li, R., Li, J., Guo, Q., Cohen, J. B., Zhai, P., Xu, X. & Hu, F. (2024). A merged continental planetary boundary layer height dataset based on high-resolution radiosonde measurements, ERA5 reanalysis, and GLDAS. *Earth System Science Data*, 16, 1-14. https://doi.org/10.5194/essd-16-1-2024

Hengl, T., Heuvelink, G. B. M. & Rossiter, D. G. (2007). About regression-kriging: From equations to case studies. *Computers & Geosciences*, 33, 1301-1315. https://doi.org/10.1016/j.cageo.2007.05.001

Hengl, T. (2009). *A practical guide to geostatistical mapping* (2nd edn.). Office for Official Publications of the European Communities, Luxembourg.

https://doi.org/10.5194/egusphere-2026-702
Preprint. Discussion started: 9 March 2026

Krähenmann, S., Walter, A., Brienen, S., Imbery, F. & Matzarakis, A. (2018). High-resolution grids of hourly meteorological variables for Germany. *Theoretical and Applied Climatology*, 131, 899-926. https://doi.org/10.1007/s00704-016-2003-7

Li, X., Dong, Y., Zhang, Y., Shi, Z. & Yao, J. (2023). Climatology of planetary boundary layer height over Jiangsu, China, based on ERA5 reanalysis data. *Atmosphere*, 14, 1330. https://doi.org/10.3390/atmos14091330

Madonna, F., Summa, D., Di Girolamo, P., Marra, F., Wang, Y. & Rosoldi, M. (2021). Assessment of trends and uncertainties in the atmospheric boundary layer height estimated using radiosounding observations over Europe. *Atmosphere*, 12, 301. https://doi.org/10.3390/atmos12030301

Nelson, K. J., Xie, F., Ao, C. O. & Oyola-Merced, M. I. (2021). Diurnal variation of the planetary boundary layer height observed from GNSS radio occultation and radiosonde soundings over the Southern Great Plains. *Journal of Atmospheric and Oceanic Technology*, 38, 2081-2093. https://doi.org/10.1175/JTECH-D-20-0196.1

Pal Arya, S. (1988). *Introduction to micrometeorology*. Academic Press, San Diego, California, USA.

Quan, J., Gao, Y., Zhang, Q., Tie, X., Cao, J., Han, S., Meng, J., Chen, P. & Zhao, D. (2013). Evolution of planetary boundary layer under different weather conditions, and its impact on aerosol concentrations. *Particuology*, 11, 34-40. https://doi.org/10.1016/j.partic.2012.04.005

Roldán-Henao, N., Su, T. & Li, Z. (2024). Refining planetary boundary layer height retrievals from micropulse lidar at multiple ARM sites around the world. *Journal of Geophysical Research: Atmospheres*, 129, e2023JD040207. https://doi.org/10.1029/2023JD040207

Saha, S., Sharma, S., Kumar, K. N., Kumar, P., Lal, S. & Kamat, D. (2022). Investigation of atmospheric boundary layer characteristics using ceilometer lidar, COSMIC GPS RO satellite, radiosonde and ERA-5 reanalysis dataset over the western Indian region. *Atmospheric Research*, 268, 105999. https://doi.org/10.1016/j.atmosres.2021.105999

Salcedo-Bosch, A., Rocadenbosch, F., Argañaraz, C. I., Curci, G. & Lolli, S. (2025). Retrieval of planetary boundary layer height from CALIPSO satellite observations using a machine learning approach. *Ecological Informatics*, 92, 103431. https://doi.org/10.1016/j.ecoinf.2025.103431

Seibert, P., Beyrich, F., Gryning, S.-E., Joffre, S., Rasmussen, A. & Tercier, P. (2000). Review and intercomparison of operational methods for the determination of the mixing height. *Atmospheric Environment*, 34, 1001-1027. https://doi.org/10.1016/S1352-2310(99)00349-0

Seidel, D. J., Ao, C. O. & Li, K. (2010). Estimating climatological planetary boundary layer heights from radiosonde observations: comparison of methods and uncertainty analysis. *Journal of Geophysical Research: Atmospheres*, 115, D16113. https://doi.org/10.1029/2009JD013680

Seidel, D. J., Zhang, Y., Beljaars, A., Golaz, J.-C., Jacobson, A. R. & Medeiros, B. (2012). Climatology of the planetary boundary layer over the continental United States and Europe. *Journal of Geophysical Research*, 117, D17106. https://doi.org/10.1029/2012JD018143

Sinclair, V. A., Ritvanen, J., Urbancic, G., Statnaia, I., Batrak, Y., Moisseev, D. & Kurppa, M. (2022). Boundary-layer height and surface stability at Hyytiälä, Finland, in ERA5 and observations. *Atmospheric Measurement Techniques*, 15, 3075-3103. https://doi.org/10.5194/amt-15-3075-2022

https://doi.org/10.5194/egusphere-2026-702
Preprint. Discussion started: 9 March 2026

Slättberg, N., Lai, H.-W., Chen, X., Ma, Y. & Chen, D. (2022). Spatial and temporal patterns of planetary boundary layer height during 1979-2018 over the Tibetan Plateau using ERA5. *International Journal of Climatology*, 42, 3360-3377. https://doi.org/10.1002/joc.7420

Stull, R. B. (1988). *An introduction to boundary layer meteorology* (1st edn.). Kluwer Academic Publishers, Dordrecht.

Teixeira, J., Piepmeier, J. R., Nehrir, A. R., Ao, C. O., Chen, S. S., Clayson, C. A., et al., (2021). Toward a global planetary boundary layer observing system: The NASA PBL Incubation Study Team report. NASA PBL Incubation Study Team, Washington, DC, USA. https://science.nasa.gov/science-ink/s3fspublic/atoms/files/NASAPBLIncubationFinalReport.pdf

Xu, Z., Chen, H., Guo, J., Zhang, G., Meng, C., Zhang, X., Hu, H., Miao, S. & Zhai, P. (2023). Regionalization of the summertime planetary boundary layer height in comparison with various reanalysis datasets over China. *Atmospheric Research*, 282, 106534. https://doi.org/10.1016/j.atmosres.2022.106534

Zhang, Y., Seidel, D. J. & Zhang, S. (2013). Trends in planetary boundary layer height over Europe. *Journal of Climate*, 26, 10071-10076. https://doi.org/10.1175/JCLI-D-13-00108.1

Zhang, H. S., Zhang, X. Y., Li, Q. H., et al.,, (2020). Research progress on estimation of the atmospheric boundary layer height. *Journal of Meteorological Research*, 34(3), 482-498. https://doi.org/10.1007/s13351-020-9910-3

Zhang, D., Comstock, J., Sivaraman, C., Mo, K., Krishnamurthy, R., Tian, J., Su, T., Li, Z. & Roldán-Henao, N. (2025). Best estimate of the planetary boundary layer height from multiple remote sensing measurements. *Atmospheric Measurement Techniques*, 18, 3453-3475. https://doi.org/10.5194/amt-18-3453-2025